ISSN 0869-5911, Petrology, 2018, Vol. 26, No. 4, pp. 414–427. © Pleiades Publishing, Ltd., 2018.
Original Russian Text © E.O. Dubinina, A.A. Borisov, 2018, published in Petrologiya, 2018, Vol. 26, No. 4, pp. 426–441.

Structure and Composition Effects on the Oxygen Isotope Fractionation in Silicate Melts

E. O. Dubinina[a], * and A. A. Borisov[a]

[a] *Institute of Geology of Ore Deposits, Petrography, Mineralogy, and Geochemistry, Russian Academy of Sciences, Moscow, 119017 Russia*

**E-mail: elenadelta@gmail.com*

Received September 18, 2017; in final form, December 5, 2017

Abstract—The influence of melt composition and structure on the oxygen isotope fractionation was studied for the multicomponent ($SiO_2 \pm TiO_2 + Al_2O_3 \pm Fe_2O_3 + MgO \pm CaO$) system at 1500°C and 1 atm. The experiments show that significant oxygen isotope effects can be observed in silicate melts even at such high temperature. It is shown that the ability of silicate melt to concentrate ^{18}O isotope is mainly determined by its structure. In particular, an increase of the NBO/T ratio in the experimental glasses from 0.11 to 1.34 is accompanied by a systematic change of oxygen isotope difference between melt and internal standard by values from −0.85 to +1.29‰. The obtained data are described by the model based on mass-balance equations and the inferred existence of O^0, O^-, and O^{2-} (bridging, non-bridging, and free oxygen) ions in the melts. An application of the model requires the intra-structure isotope fractionation between bridging and non-bridging oxygens. Calculations show that the intra-structure isotope fractionation in our experiments is equal to 4.2 ± 1.0‰. To describe the obtained oxygen isotope effects at the melts relatively to temperature and fraction of non-bridging oxygen a general equation was proposed.

Keywords: oxygen isotopes, fractionation, silicate melt, NBO/T ratio, bridging, non-bridging, isotope equilibrium, experiment

DOI: 10.1134/S0869591118040021

INTRODUCTION

Oxygen isotope thermometry and geochemistry are widely used to detect the sources, extent of crustal contamination, crystallization conditions, and cooling dynamics of silicate melts. Available data on the equilibrium oxygen isotope fractionation between rock-forming minerals can be used to estimate the closure temperature within domains of crystalline rocks. These data also can be used to detect the opening of oxygen isotope system during the fluid–rock interaction. Estimation of isotope equilibria in the phenocryst–melt system of volcanic rocks makes it possible to reconstruct magma generation processes, dynamics of melt cooling or evaluate the contribution of contamination.

Oxygen isotope thermometry is based on the experimental and theoretical calibrations of oxygen isotope fractionation coefficients between minerals at the geologically significant temperatures (usually, from 600 to 1200°C, Chacko et al., 2001). However, the interpretation of melt-bearing magmatic systems is complicated by a poor knowledge of oxygen isotope fractionation in silicate melts. Fragmentary experimental data were obtained for melts of different chemical composition and for different temperatures. It is difficult to systematize the experimental calibrations and to applicate the calibrations to natural silicate melts with the complex composition. Extrapolation of experimental results to natural melts is complicated by the absence of reliable theoretical description of the structure of silicate melts (Appora et al., 2003; Ariskin and Polyakov, 2008). Usually this problem is solved by diverse approximations of silicate melts, more frequently, by the calculation for normative mineral composition. Then, the weighted average fractionation coefficient is calculated for melts using the weighted average fractionation factors of individual minerals (e.g., Bucholz et al., 2017; Eiler, 2001). Less common is using of half-empirical chemical indices. For example, $I^{18}O$-index was applied for calculation of the phenocryst-lava oxygen isotope fractionation (Zhao and Zheng, 2003). The Garlick index can be termed both as chemical and structure index (Garlick, 1966). The index is based on the positive link between the ^{18}O concentration and SiO_2 and Al_2O_3. Also it is based on the negative correlation with some other rock-forming oxides.

Some approximations which were applied to predict the oxygen isotope fractionation in magmatic systems were testified experimentally (Appora et al., 2003; Borisov and Dubinina, 2014). However, the

range of compositions in these works was insufficiently wide to select the most suitable way of approximation. At the same time, the experiments at 1500°C with the diopside–anorthite eutectic melts modified by Fe, Ti, and Al oxides (Borisov and Dubinina, 2014) clearly show that the oxygen isotope fractionation depends on the proportions of network-forming and network-modifying cations expressed by NBO/T ratio. As a first approximation, this parameter describes the melt structure or polymerization extent and it is calculated as the ratio of non-bridging oxygens to tetrahedral cations (Mysen et al., 1985; Mysen and Richet, 2005, etc.). According to (Borisov and Dubinina, 2014), oxygen atoms located at the different sites have different concentrations of ^{18}O isotope. So, the melts with the different polymerization should differ in their ability to concentrate heavy oxygen isotope (Qin et al., 2016).

It is known that the Si–O bond is always enriched in heavy oxygen compare to Me–O one (Garlick, 1966; Clayton and Kieffer, 1991; Zheng, 1991, 1993, etc.). Since silica is the network-former, the structure indices (NBO/T or Garlick index) should correlate with the degree of melt enrichment in heavy oxygen. In natural melts, this relation is observed as generally known tendency to increase of $\delta^{18}O$ values from mafic to felsic rocks, i.e. from less to more polymerized melts (Garlick, 1966). However, experimental attempts to confirm the influence of melt structure on the oxygen isotope fractionation are controversial. For instance, experiments with immiscible high-Fe and high-Si melts in the presence of water fluid at 1100–1200°C (Lester et al., 2013) show no influence of the NBO/T ratio on the oxygen isotope fractionation. However, for felsic melts and Ne-melilite melt at $900 < T < 1400$°C (Appora et al., 2003) good correlation of oxygen isotope fractionation coefficients with the Garlick index was obtained.

According to the theoretical basis (Bigeleisen and Mayer, 1947), isotope fractionation at high temperatures is negligible even for light elements. For oxygen isotopes the estimates of $10^3 Ln\alpha$ value between rhyolite and basalt at 1500°C are 0.39 or 0.78‰ according to increment method (Zhao and Zheng, 2003) or extrapolated experimental data (Appora et al., 2003). The present-day analytical precision of oxygen isotope analysis of silicates ($<\pm 0.1$‰) can provide the accuracy for determination of these isotope effects. However, significant isotope effects in melt-bearing systems were obtained at recent experiments for other light elements (H, N, S). Large isotope effect was recorded by Raman spectroscopy and NMR for ^1H and ^2H isotopes bounded with variably polymerized silicate tetrahedra (Le Losq et al., 2016). Significant intramolecular hydrogen isotope partitioning was found in hydrated silicate melts at 1400°C (Wang et al., 2015). Similar data were obtained for silicate melts and aqueous fluid not only for $^2H/^1H$, but also for $^{15}N/^{14}N$ (Dalou et al., 2015; Mysen, 2013; Mysen and Fogel, 2010) and $^{34}S/^{32}S$ (Labidi et al., 2016) ratios. All these authors noted that the value of observed isotope effects at high temperatures is mainly determined by melt structure.

It should be noted that the isotope ratios in the cited works were estimated using spectroscopic methods. The mass-spectrometric measurements of oxygen isotope fractionation between silicate melts are few and did not show significant isotope effects yet. Among these experiments are single works on study of immiscible melts (Kyser et al., 1998; Lester et al., 2013). Most experimental studies of the equilibrium oxygen fractionation in melt-bearing systems were carried out by isotope equilibration with gas phase, usually, CO_2 (Stolper and Epstein, 1991; Palin et al., 1996; Matthews et al., 1994; Appora et al., 2003). Some information on the equilibrium oxygen isotope fractionation can be obtained from experimental assessment of oxygen diffusion rates in silicate melts (Muehlenbachs and Kushiro, 1974; Canil and Muehlenbachs, 1990; Dunn, 1982; Wendlandt, 1991, etc.). But in general, experimental studies of the oxygen isotope fractionation in systems involving silicate melts are insufficient for systematic description of natural melts with wide variations of chemical composition. A special study of oxygen isotope fractionation at the silicate melts was carried out at 1400–1570°C (Borisov and Dubinina, 2014). The work was focused on the effect of melt composition. Significant isotope fractionation (up to 1.5‰) caused by difference in the content of network-forming cations was found at 1500°C. These results stimulated the further experiments, which are the subject of this paper.

The special study of oxygen isotope fractionation in silicate melts was carried out at the same temperature (1500°C) within much wider range of NBO/T ratios. To reach maximum NBO/T variations, we used different eutectic compositions doped with network-forming (Si^{4+}, Ti^{4+}, Al^{3+}, Fe^{3+}) and network-modifying (Ca^{2+}, Mg^{2+}, Fe^{2+}) cations. Thus, we covered a wide range of chemical compositions in the multicomponent system $SiO_2 \pm TiO_2 + Al_2O_3 \pm Fe_2O_3 + MgO \pm CaO$. A large pool of experiments was carried out to apply statistic treatment, for example, to estimate reliably applicability of chemical and structural indices.

The validity of applied experimental technique was tested on the diopside–anorthite eutectic melts modified by Fe, Ti, and Al oxides (Borisov and Dubinina, 2014). The technique is the simultaneous isotope equilibration of different silicate melts with the same gas under the same conditions. If each melted sample reaches the oxygen isotope equilibrium with ambient gas during the experiment, one can say that any two melts are equilibrated with each other. So, the melt–melt partition coefficients obtained in such experiments are identical to those between the immiscible melts. However, as compared to experiments with liq-

uid immiscibility, isotope equilibration through an ambient gas excludes any cross contamination of melts and is very suitable for study of large experimental samples (few mg) with any chemical compositions.

METHODS

Experiments were carried out in a vertical tube furnace in air at a pressure of 1 atm. In each run several silicate melts together with a melt of diopside–anorthite eutectic composition (DA) were equilibrated with the same ambient gas. This DA composition was taken as an internal standard required for comparison of experiments. Similar approach was used in the experimental study of $\delta^{15}N$ and δD values in silicate melts (Mysen and Fogel, 2010). As shown, the use of a melt as an internal standard makes it possible to avoid the control of $\delta^{18}O$ value of a gas phase (Borisov and Dubinina, 2014).

Prepared compositions of experimental mixtures cover a wide range of NBO/T ratio (0.11–1.38). Three synthetic iron-free compositions were taken as the base compositions: diopside–anorthite eutectic (DA), felsic enstatite–anorthite–silica eutectic (HR), and Ca-free eutectic in the $MgO–Al_2O_3–SiO_2$ system (HA). In order to obtain Fe-bearing compositions (DAF), the DA composition was doped with 10 wt % Fe_2O_3, while more felsic Fe-rich compositions (DAFS) were obtained by SiO_2 introduction in DAF composition. The DAF and DAFS compositions are analogues of haplobasalt and haplorhyolite. Other compositions were obtained by addition of TiO_2 (DAFT, DAFST), Al_2O_3 (DAFA, DAFSA), or MgO (DAFM, DAFSM). In order to obtain melts with different Fe content (DAF5 and DAF20), the DA composition was doped with 5 and 20 wt % Fe_2O_3. The DAFOL composition was prepared by addition of powdered San Carlos olivine to the DAF composition. In the Ca-free system (HA), the Fe-bearing composition was obtained by doping with 10 wt % Fe_2O_3 (HAF), while further modification of this system was performed by addition of different amounts of CaO (HAFC compositions). Brief characteristics of the compositions are given in Table 1. All Fe-bearing compositions were initially prepared to study the effect of melt composition on the Fe^{3+}/Fe^{2+} ratio. Therefore, many experimental details and technique of determination of redox ratio in experimental glasses can be found in the corresponding works (Borisov et al., 2013, 2015, 2017).

Experimental isotope equilibration of melts was performed by a loop technique (Borisov, 2001). The loop 1.5 mm across was prepared from platinum wire (0.125 mm, Pt 99.9%, Chempur®). A mixture of corresponding composition was homogenized by powdering, then mixed with an aqueous solution of polyvinyl alcohol to a cohesive mass, and applied to a loop. Obtained loops filled with required compositions were suspended on a ceramic holder and loaded into tube furnace. The temperature was measured by $Pt/PtRh_{10}$ thermocouple calibrated relative to melting points of Au (1064°C) and Pd (1553°C) with an accuracy of ±2°C. In total, we conducted five runs at 1500°C in air. In each run, from four to ten samples of different composition, including DA composition, were brought in isotope equilibrium with atmospheric oxygen (Table 1).

To be sure that all melts reached oxygen isotope equilibrium with ambient atmosphere, the experimental time was taken long enough to provide the isotope equilibrium of a spherical melt drop 0.075 cm across with atmosphere oxygen by diffusion. Calculation shows that at oxygen diffusion rate of around 5×10^{-8} cm^2 s^{-1} (at 1500°C, Lesher, 2010), 42 hours are required for 99.9% diffusion exchange of felsic melt with ambient oxygen. Much less time is required to reach equilibrium for basic melt due to its lower viscosity (Mungall, 2002). According to our experimental data, oxygen isotope equilibration between 1.5-mm drops of Fe-bearing haplogranite and haplobasalt melts was reached for less than 60 h at 1400°C and for only 25 h at 1500°C (Borisov and Dubinina, 2014). It is possible that the attainment of equilibrium is additionally accelerated by convection that uninterruptedly homogenizes a melt within a loop during experiment (Borisov, 2001). In this work, the duration of all experiments fulfills both theoretical and experimental estimates of time required to reach oxygen isotope equilibrium between melts (42–45.5 h, Table 2).

After experiment, the sample holder was withdrawn from a furnace. Small size of melt drops provided practically instant quenching. To prepare for the oxygen isotope analysis, samples were extracted from loop and crushed into fragments.

Results of 67 series performed at the same conditions and by the same method (Borisov and Dubinina, 2014) were also included in Table 2.

Oxygen Isotope Analysis

The oxygen isotope analysis of experimental glasses was carried out by laser fluorination technique (Sharp, 1990). The 1–2 mg of unknown samples and standards were dispersed into the stainless-steel chamber covered by BaF_2 glass. The chamber was evacuated to 10^{-3}–10^{-4} mbar and filled with BrF_5 to remove residual moisture from surfaces of chamber and samples. After the preliminary fluorination, samples were subsequently decomposed in the BaF_5 atmosphere by a local heating with a 30W CO_2 laser. Obtained gas was purified by cryogenic traps and supplied into the dual inlet system of DELTAplus mass spectrometer (Thermo, Germany). Ion currents of 32, 33 and 34 m/z were measured relative to O_2 working standard. The standard was calibrated at the V-SMOW scale using the oxygen released from two international standards:

Table 1. Composition and calculated chemical and structural indices of the studied melts

Melt composition	SiO_2	TiO_2	Al_2O_3	Fe_2O_3	MgO	CaO	Total	Fe^{3+}/Fe^{2+}	λ_{th}	λ_{corr}	$I^{18}O$	I^G	NBO/T	X_{nb}
DA	50.6	0.0	15.7	0.0	10.1	23.6	100.0	–	0.604	0.581	0.807	0.693	0.901	0.368
DAF5	48.0	0.0	15.0	4.7	9.6	22.6	99.9	1.8	0.610	0.588	0.797	0.681	0.875	0.359
DAF20	40.4	0.0	12.7	19.4	8.1	19.0	99.6	2.3	0.630	0.611	0.762	0.640	0.737	0.311
DAF	45.6	0.0	14.1	9.8	9.1	21.3	99.9	1.9	0.617	0.596	0.785	0.669	0.838	0.346
DAFS	66.1	0.0	7.6	10.0	4.9	11.4	99.9	1.4	0.558	0.546	0.877	0.820	0.401	0.182
DAFM15	42.8	0.0	13.3	9.8	14.7	19.8	100.3	2.3	0.626	0.607	0.761	0.629	1.102	0.432
DAFM20	39.9	0.0	12.4	9.7	19.8	18.5	100.4	2.8	0.603	0.579	0.737	0.591	0.392	0.512
DAFSM13	60.6	0.0	6.9	10.1	12.9	10.2	100.6	1.4	0.574	0.564	0.839	0.758	0.737	0.311
DAFSM21	54.4	0.0	6.3	10.1	20.7	9.2	100.7	1.5	0.592	0.583	0.798	0.693	1.142	0.444
DAFOL20	45.5	0.0	12.6	8.8	15.0	18.6	100.5	2.1	0.618	0.600	0.772	0.647	1.075	0.424
DAFOL40	44.7	0.0	10.4	9.3	21.0	15.4	100.9	2.2	0.621	0.606	0.755	0.622	1.344	0.503
DAFA22	41.1	0.0	21.7	9.7	8.1	19.0	99.6	1.9	0.616	0.583	0.793	0.659	0.553	0.243
DAFA30	36.1	0.0	29.3	10.0	7.0	16.8	99.3	1.9	0.616	0.570	0.798	0.646	0.302	0.141
DAFSA15	60.0	0.0	14.9	9.7	4.3	10.3	99.2	1.2	0.562	0.538	0.876	0.799	0.245	0.115
DAFSA23	54.1	0.0	22.3	9.8	3.9	9.3	99.4	0.9	0.567	0.536	0.872	0.776	0.112	0.055
DAFT10	40.8	9.3	12.5	9.4	8.1	18.9	99.0	1.8	0.617	0.598	0.771	0.608	0.752	0.316
DAFT20	35.0	19.5	10.8	9.5	7.0	16.4	98.2	1.7	0.618	0.602	0.752	0.535	0.659	0.283
DAFT30	30.4	28.4	9.4	9.6	6.1	14.3	98.2	1.6	0.620	0.605	0.736	0.470	0.579	0.253
DAFST15	55.9	14.2	6.2	9.3	4.0	9.5	99.2	1.3	0.565	0.555	0.846	0.714	0.349	0.161
DAFST25	48.3	24.6	5.4	9.7	3.4	8.3	99.7	1.2	0.573	0.564	0.818	0.628	0.316	0.146
DA/DAFT10	45.0	5.2	14.1	5.2	9.0	20.4	98.9	1.8	0.610	0.589	0.789	0.649	0.799	0.333
DA/DAFA20	45.9	0.0	18.4	4.6	9.3	21.2	99.4	1.9	0.609	0.582	0.800	0.677	0.736	0.311
DA/DAFSA21	52.8	0.0	18.2	4.9	7.2	16.4	99.6	1.5	0.585	0.557	0.840	0.736	0.470	0.210
HA	61.8	0.0	17.8	0.0	20.5	0.0	100.0	–	0.550	0.536	0.872	0.764	0.484	0.216
HAC	50.4	0.0	14.7	0.0	16.9	17.8	99.9	–	0.600	0.579	0.800	0.677	1.049	0.416
HAF	56.1	0.0	16.1	10.0	18.6	0.0	100.9	0.9	0.566	0.566	0.847	0.740	0.516	0.229
HAFC5	52.5	0.0	15.1	10.6	17.3	5.4	100.9	1.2	0.581	0.563	0.825	0.712	0.648	0.279
HAFC11	49.3	0.0	14.1	9.9	16.3	10.9	100.5	1.5	0.597	0.576	0.803	0.685	0.806	0.335
HAFC16	45.9	0.0	13.2	10.1	15.1	16.4	100.6	1.8	0.614	0.595	0.779	0.655	0.984	0.395
HAFS	64.3	0.0	12.3	10.1	14.2	0.0	100.9	0.9	0.549	0.539	0.878	0.797	0.392	0.179
HAFC5S	63.2	0.0	10.9	10.0	12.6	3.9	100.7	1.0	0.556	0.543	0.868	0.789	0.460	0.206
HAFC11S	61.5	0.0	10.1	9.6	11.6	7.7	100.5	1.2	0.565	0.550	0.857	0.776	0.542	0.239
HAFC16S	60.2	0.0	9.0	9.9	10.3	11.1	100.4	1.3	0.573	0.559	0.847	0.767	0.613	0.266
HR	63.3	0.0	12.5	0.0	11.8	12.4	100.0	–	0.563	0.544	0.864	0.776	0.602	0.261
HRF5	60.1	0.0	12.0	5.6	11.2	11.8	100.8	1.3	0.571	0.553	0.850	0.762	0.600	0.261
HRF10	57.5	0.0	11.4	9.8	10.7	11.3	100.8	1.4	0.578	0.560	0.840	0.750	0.590	0.257
HRF20	51.3	0.0	10.1	19.9	9.5	10.0	100.7	1.6	0.593	0.578	0.813	0.721	0.558	0.245

Oxide contents are given in wt %, Fe_2O_3 is the total iron. Indices NBO/T, λ_{th} , and λ_{corr} were calculated after (Mills, 1993).

Table 2. Oxygen isotope composition and value of isotope fractionation $\Delta^{18}O$ (L–DA) in experimental glasses

Run 77 (43 h)	Sample	DA	DAF	DAFM15	DAFM20	DAFS	DAFSM13	DAFSM21	DAFOL20	DAFOL40		
	$\delta^{18}O$, ‰	22.37	22.60	21.70	21.66	22.86	22.54	21.82	22.34	21.52		
	$\Delta^{18}O$ (L-DA), ‰		0.22	−0.68	−0.72	0.48	0.17	−0.56	−0.04	−0.85		
Run 12 (46 h)	Sample	DA	HR	HRF5	HRF10	HRF20						
	$\delta^{18}O$, ‰	22.16	22.64	22.90	22.62	22.82						
	$\Delta^{18}O$ (L-DA), ‰		0.49	0.74	0.47	0.66						
Run 5 (45 h)	Sample	DA	HA	HAC	HAF	HAFC5	HAFC11	HAFC16	HAFS	HAFC5S	HAFC11S	HAFC16S
	$\delta^{18}O$, ‰	21.96	22.96	21.84	23.16	22.75	22.56	22.06	23.25	22.94	22.30	22.65
	$\Delta^{18}O$ (L-DA), ‰		1.00	−0.12	1.20	0.79	0.60	0.10	1.29	0.98	0.34	0.69
Run 78 (43 h)	Sample	DA	HR	DAFS	DAFSA15	DAFSA23	DAFST15	DAFST25	DA/DAFT10	DA/DAFA20	DA/DAFSA21	
	$\delta^{18}O$, ‰	21.79	22.18	22.52	22.48	22.98	22.65	22.75	22.17	21.97	22.54	
	$\Delta^{18}O$ (L-DA), ‰		0.39	0.73	0.69	1.20	0.87	0.96	0.38	0.18	0.76	
Run 67* (42 h)	Sample	DA	DAF5	DAF	DAF20	DAFT10	DAFT20	DAFA22	DAFT30	DAFA30		
	$\delta^{18}O$, ‰	12.73	12.71	12.87	13.12	12.91	13.00	13.23	12.82	13.00		
	$\Delta^{18}O$ (L-DA), ‰		−0.02	0.14	0.39	0.18	0.27	0.50	0.09	0.27		

* Data from (Borisov and Dubinina, 2014).

NBS-28 (quartz, $\delta^{18}O = 9.58‰$) and UWG-2 (garnet, $\delta^{18}O = 5.80‰$, Valley et al., 1995). The internal (quartz POLARIS) and international (NBS biotite and San Carlos olivine) standards were decomposed in each measurement series. The $\delta^{18}O$ values $5.16 \pm 0.10‰$ and $5.27 \pm 0.10‰$ were obtained for the biotite NBS-30 ($n = 8$, recommended value of 5.10‰, Coplen, 1994) and for the San Carlos olivine ($n = 18$). The accuracy $\delta^{18}O$ measurements better than $\pm 0.10‰$ (1σ) was estimated using the repeated measurements of the standards and replicates.

A methodical problem was detected with the analysis of very high silica glasses. Some of them starts react with the BrF_5 at room temperature. This excludes not only the stage of preliminary fluorination, but also the subsequent analysis of several samples loaded in one chamber. Heating of any sample is accompanied by uncontrolled contamination with oxygen released from other samples. For the samples instable to fluorides we applied the bracketing standard technique.

We prepared the small Ni holder with three cells. Two of them were filled by internal quartz standard POLARIS ($\delta^{18}O = 13.0 \pm 0.10‰$) and one of them was filled by unknown sample. This holder was placed in the reaction chamber. After that the chamber was evacuated and pre-fluorinated very shortly. After that the subsequent laser fluorination of standard, unknown sample, and again standard was done. The $\delta^{18}O$ value of unknown sample was corrected to $\delta^{18}O$ of the internal standard. The method was tested several times by the measurement of oxygen isotope composition of well-known samples. The reproducibility of $\delta^{18}O$ was $\pm 0.15‰$, which is close to the accuracy of laser fluorination technique. The results are given in Table 2.

Microprobe Analysis and Determination of Fe^{3+}/Fe^{2+} Ratio

The bulk chemical composition of experimental glasses was determined by EPMA method on a Cameca SX100 (Institute of Mineralogy, LUH, Germany) at an accelerating voltage of 15 kV, ion current of 15 nA, and counting time of 10 s. Each sample was analyzed in 20 points, and obtained data were averaged.

The Fe^{3+}/Fe^{2+} ratio in the Fe-bearing glasses was studied in similar experiments (Borisov et al., 2013, 2015, 2017). For each type of glasses obtained at 1500°C all available Fe^{3+}/Fe^{2+} values were averaged (e.g., on eight measurements for DAF glasses and on six analyses for DAFS glasses). In rare cases, the redox ratio at 1500°C was calculated by extrapolation of data available for lower temperatures. The measurement error of Fe^{3+}/Fe^{2+} ratio is ≈0.1. A complete description of the measurement procedure of di- and trivalent iron in experimental glasses is given in (Schuessler et al., 2008).

RESULTS

All $\delta^{18}O$ values measured in experimental glasses are close to the isotope composition of atmospheric oxygen (+23.5‰, Kroopnick and Craig, 1972), which is expectable for experiments performed in air without forcible flushing of the furnace by a gas. The exception is series 67, where isotope composition of atmospheric oxygen was significantly changed presumably by the thermal diffusion (see Discussion in paper by Borisov and Dubinina, 2014). However, different oxygen isotope composition of ambient atmosphere in different runs is leveled by normalization of oxygen isotope fractionation relative to internal standard DA, which was present in all runs (series):

$$\Delta^{18}O(\text{L-DA}) = \delta^{18}O(\text{L})_n - \delta^{18}O(\text{DA})_n,$$

where n is the run number, $\delta^{18}O(L)_n$ and $\delta^{18}O(DA)$ are the oxygen isotope composition of a melt L and of the DA, which are the products of the same run. This isotope fractionation is listed in Table 2 together with measured $\delta^{18}O$ values in experimental glasses. Total variations of $\Delta^{18}O(L-DA)$ are 2.1‰ (from −0.85 to +1.29‰). Below we report the description of the effect of individual oxides on the $\Delta^{18}O(L\text{-}DA)$. However, it should be taken into account that addition of an oxide is accompanied by the proportional decrease of contents of other oxides, i.e., the observed isotope effect is controlled not only by input, but also by removal of definite elements.

Effect of Addition of Iron Oxides

Figure 1a shows the effect of the total Fe_2O_3 content on the oxygen isotope fractionation in three pseudobinary systems: DA + Fe_2O_3, HR + Fe_2O_3, and HA + Fe_2O_3. It should be noted that the Fe^{3+}/Fe^{2+} ratio in the Fe-bearing melts is not constant and varies from 0.9 to 1.9 (exact values are given in Table 1). In general, an increase of Fe_2O_3 content leads to the increase of $\Delta^{18}O(L\text{-}DA)$. This effect is moderate in the DA + Fe_2O_3 and HR + Fe_2O_3 systems and strong in the HA+Fe_2O_3 system.

Effect of the CaO and MgO Addition

Figure 1b shows variations of $\Delta^{18}O(L\text{-}DA)$ depending on the CaO content in the pseudobinary systems HA + CaO, HAF + CaO, and HAFS + CaO. This effect is very significant. For example, the increasing of the CaO content from 0 to 16.4 wt % in the system HAFS + CaO leads to decreasing of $\Delta^{18}O(L\text{-}DA)$ by 1.1‰, which is ten times higher than analytical error.

The effect of the MgO content on the oxygen isotope fractionation was studied in three pseudobinary systems: basic DAF + MgO, felsic DAFS + MgO, and basic olivine-bearing DAF + ScOL ones (Fig. 1c). In experiments with addition of natural San Carlos olivine, an increase of MgO content is accompanied by

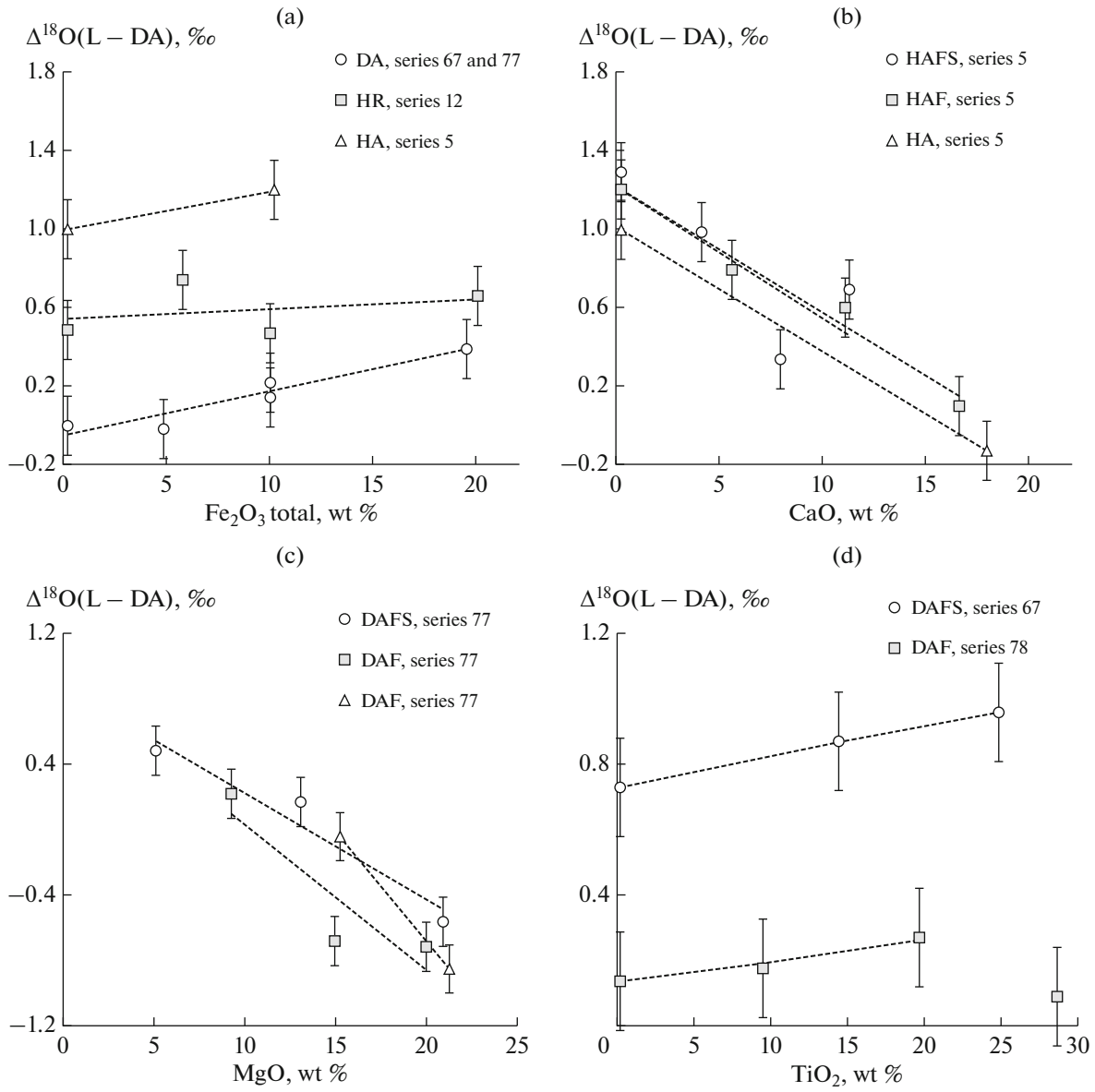

Fig. 1. Oxygen isotope fractionation in silicate melts relative to the basic melt (DA) versus the content of added oxides: (a) iron, (b) calcium, (c) magnesium, (d) titanium. Different symbols in the diagrams correspond to different base eutectics doped with oxides.

the proportional growth of silica content, which is present in olivine, however experimental points for DAF + ScOL compositions are confined to the general trend. This implies that an increase of MgO content (like the CaO) in silicate melt results in the moderate decrease of $\Delta^{18}O(L-DA)$.

Effect of Addition of SiO_2, TiO_2, and Al_2O_3

The effect of TiO_2 content on the oxygen isotope fractionation is shown in Fig. 1d for two pseudobinary systems: DAF + TiO_2 and DAFS + TiO_2. Ignoring the sample (DAFT30) with the extremely high Ti content, it is seen that an increase of TiO_2 in silicate melts results in the moderate increase of $\Delta^{18}O(L\text{-}DA)$.

An increase of Al_2O_3 content in two pseudobinary systems DAF + Al_2O_3 and DAFS + Al_2O_3 results in the insignificant increase of $\Delta^{18}O(L\text{-}DA)$, although some scatter of data indicates more complex behavior of oxygen isotopes doped with Al_2O_3 as compared to the TiO_2-doped systems.

It is seen in Fig. 1d that $\Delta^{18}O(L\text{-}DA)$ in felsic compositions (DAFS) are approximately 0.6‰ higher than those of basic compositions (DAF), which pre-

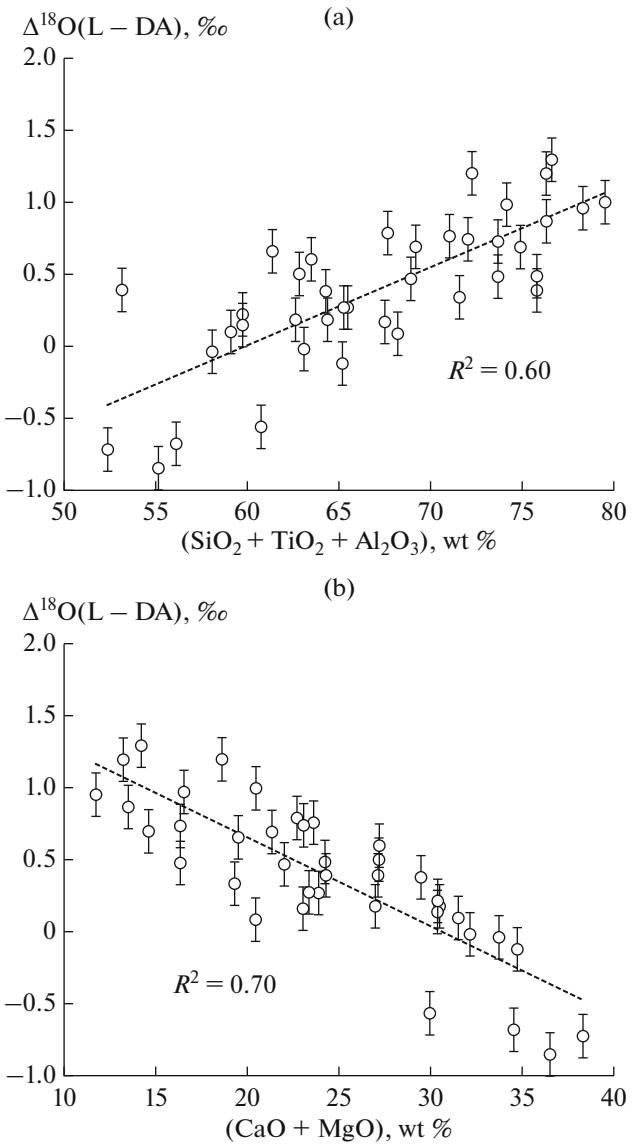

Fig. 2. Oxygen isotope fractionation in silicate melts relative to the basic melt (DA) depending on the total content of network-forming (a) and network-modifier (b) cations.

sumably reflects an effect of elevated silica content facilitating the enrichment of a melt in heavy oxygen.

DISCUSSION

Oxygen Isotope Fractionation and Element Composition of a Melt

Obtained $\delta^{18}O$ variations in experimental melts are clearly beyond the analytical errors and exceed any estimates obtained using classical methods by extrapolation to the studied temperature interval. For example, the extrapolation of the phenocryst-lava equations (Zhao and Zheng, 2003) gives the difference between rhyolite and basalt near 0.4‰ at 1500°C. Extrapolation of equation (Appora et al., 2003) to this temperature gives 0.8‰.

Our results show that chemical composition of silicate melts essentially affects their ability to concentrate ^{18}O (Fig. 1). This is expectable result, since the relation between oxygen isotope fractionation in silicate rocks was proposed in the model by (Garlick, 1966) as follows:

$$I^G = (C_{Si} + 0.58C_{Al})/\Sigma C_i,$$

where C_{Si}, C_{Al} and C_i are the molar concentrations of oxygen bound with Si, Al, and *i*th cation, respectively, while I^G is the Garlick index showing the rock enrichment in ^{18}O. Ability of silicate melts to concentrate heavy oxygen isotope can be estimated using approach based on the calculation of half-empirical index $I^{18}O$ (Zhao and Zheng, 2003). As follows from estimates based on chemical indices, melts enriched in SiO_2 and Al_2O_3 are more enriched in ^{18}O compare to basic melts. The same conclusion was obtained using approximation of melts by normative mineral composition, with subsequent calculation of the bulk weighted average fractionation coefficient (e.g., Eiler, 2001; Bucholz et al., 2017).

However, the oxygen isotope fractionation coefficients for minerals were estimated only for temperature <1200°C (e.g., Chacko et al., 2001; Zhao, Zheng, 2003). In this work, the experiments were carried out at temperature which is 300°C higher. However, oxygen isotope fractionation obtained shows the same links, which are predicted by extrapolation using methods presented above. In general, the contents of Si, Al, Ti, and trivalent Fe correlate positively with the $\Delta^{18}O$(L-DA) value, while Ca and Mg contents, in contrast, show negative correlation with this value. The former elements are the network-formers, while the last elements are the network-modifiers. Hence, the presence of network-forming and modifier cations leads to the enrichment and depletion in heavy isotope ^{18}O, respectively (Fig. 2).

Among generally accepted parameters, which reflect the proportions of oxygen atoms in different structural position the NBO/T is calculated with allowance for the oxygen bound with modifier and network-forming cations (Mysen et al., 1985; Mysen and Richet, 2005, etc.). Correspondingly, experimental data obtained show strong correlation between $\Delta^{18}O$(L-DA) and NBO/T ratio (Fig. 3).

Calculation of NBO/T ratio involves only total oxygen content bound with definite cation type (metal-modifiers and forming tetrahedra), i.e., it does not take into account proportions of cations ascribed to the same type (e. g., fraction of Si and Ti in the total content of network-forming cations). Significant correlation observed for experimental trend in Fig. 3 implies that the effect of proportions of cations allocated in different structural positions prevails over the

effect of the chemical composition of melt on the concentration of heavy oxygen isotope.

However, the melt structure is determined by its chemical composition and it is difficult to prove which of these two factors more significantly affects the oxygen isotope fractionation. For example, the known parameter "theoretical optical basicity", λ_{th} (e.g., Duffy, 1993), takes into account the differences between all constituent oxides and is calculated as $\Sigma\lambda_i X_i$, where λ_i and X_i are the basicity and equivalent fraction of each oxide in a melt, respectively. Complex aluminosilicate melts are also described by "corrected optical basicity," λ_{corr}, which takes into account that some of alkaline and alkali earth cations can be involved to compensate Al^{3+} (Mills, 1993). Both these parameters are chemical indices. It was shown that the model based on λ_{corr} satisfactory describes the sulfide capacity of slags (Hao and Wang, 2017). However, the isotope fractionation results in the weak correlation with λ_{corr} and λ_{th}. Similar estimates were obtained for correlation coefficients between $\Delta^{18}O$(L-DA) and another chemical index, $I^{18}O$ (Table 3). A weak correlation is also observed for the Garlick's index, which is, however, likely related to the imperfectness of its formulation, in particular, the underestimated role of structural position of oxygen. As demonstrated by the correlation coefficients presented in Table 3, oxygen isotope fractionation in melts has a strong correlation only with NBO/T ratio. This denotes, on the one hand, that structural position of oxygen plays significant role in the isotope fractionation, and, on the other hand, that silicate melts reveal intra-structure fractionation of oxygen isotopes.

Intra-structure Fractionation of Oxygen Isotopes in Silicate Melts

Obtained data were described by the model assuming that silicate melt at given *P-T* parameters is characterized by equilibrium partitioning of oxygen ions of three types: ions forming single bond (O^-, or "non-bridging"), double bond (O^0, or "bridging"), and "free" oxygen (O^{2-}) (Toop and Samis, 1962; Masson, 1968; Masson et al., 1970; Esin, 1975; Anfilogov et al., 2005). According to the charge conservation law, the equilibrium distribution of different oxygen particles can be described by the polymerization reaction (Fincham and Richardson, 1954; Hess, 1971):

$$2O^- \leftrightarrow O^0 + O^{2-}. \quad (1)$$

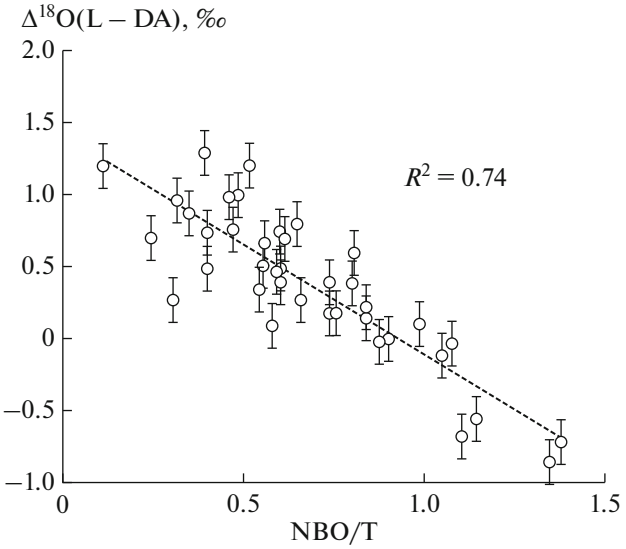

Fig. 3. Oxygen isotope fractionation in silicate melts relative to (DA) depending on the NBO/T ratio.

As a first approximation, we may suggest that the entire oxygen in our experimental melts is represented by two types: bridging (O^0) and non-bridging (O^-). This approximation is true, because O^{2-} concentration in melts containing > 40 wt % SiO_2 is negligible (Moretti, 2005; Hess, 1971). This condition is fulfilled for all studied melts, except for three melts with high Al_2O_3 and TiO_2 contents (DAFA30, DAFT20, and DAFT30, Table 1). The second assumption is that the oxygen isotope equilibrium between a melt and ambient gas takes place in our runs, as was discussed above. Assuming the intra-structure isotope fractionation between bridging (b) and non-bridging (nb) oxygen in the same melt, it is reasonable to expect that the oxygen isotope composition of melt depends on the mole fraction of oxygen ions of different types: X_b and X_{nb} ($X_b + X_{nb} \approx 1$). If intra-structure fractionation of oxygen isotopes is equilibrium, the isotope fractionation coefficient between bridging and non-bridging oxygens ($\alpha_{b\text{-}nb}$) would be constant at the same temperature and independent on other factors. Of course, this is a simplified approach, which does not take into account that non-bridging oxygen could be related to different modifier cations, while bridging oxygen, to different network-forming cations. In addition, the possible affiliation of oxygen ions to tetrahedra with

Table 3. Correlation coefficient (R^2) of oxygen isotope fractionation $\Delta^{18}O$(L-DA) vs. chemical and structural indices

Parameter	Fe^{3+}/Fe^{2+}	NBO/T	X_{nb}	λ_{th}	λ_{corr}	$I^{18}O$	I^G
n (number of points)	35	39					
R^2	0.64	0.75	0.73	0.55	0.57	0.55	0.31

different number of non-bridging oxygen (different Q particles) is also ignored. At the same time, as it will be shown below, this approach satisfactorily describes obtained experimental data.

Significant correlation of experimental $\Delta^{18}O$(L-DA) values with NBO/T (Table 3), which is better than correlation with other indices and parameters (I^G, $I^{18}O$, λ_{th}, and λ_{corr}), indicates a non-zero fractionation coefficient between bridging and non-bridging oxygens and supports the assumption that the bridging versus non-bridging oxygen is the main reason for the intra-sructure isotope effect.

One more strong argument in support the intra-structure isotope fractionation was found from the experimental series, which were doped with only one definite cation at the expense of the proportional decrease of content of most other cations. For these series, oxygen isotope fractionation should be calculated relative to corresponding starting melts compositions (for instance, in samples DAFT15 and DAFT25 relative to DAF or in samples HRF5, HRF, and HRF20 relative to HR), not to DA.

In samples doped with oxides of network-forming cations (TiO_2, Al_2O_3 and Fe_2O_3), the observed oxygen isotope fractionation relative to starting compositions DAF, DAFS, and HR were insignificant, within analytical error, in spite of the wide range of dopings (Fig. 4). Only increase of Ti and Al oxides more than 20 wt % resulted in the increase of isotope fractionation by value exceeding the analytical error. At the same time, the addition of network-modifier cations (Ca and Mg) to the corresponding starting compositions HAF, HAFS, DAF, and DAFS caused a significant oxygen isotope fractionation (Fig. 5). In the same manner, the addition of modifier cations causes a stronger change of NBO/T value compare to network-forming cations.

It is worth to mention that the value of the chemical index $I^{18}O$ in the experimental series shown in Fig. 4 changed significantly, because silica ($I^{18}O = 1.0000$) predominant in the melt was partially substituted for TiO_2 or Fe_2O_3 ($I^{18}O = 0.6322$ and 0.4809, respectively, Zhao and Zheng, 2003). However, a change of $I^{18}O$ index did not affect the oxygen isotope fractionation relative to the starting melt.

Mass Balance in Melts

According to mass-balance conditions, when melt reaches isotope equilibrium with ambient gas, the contents of ^{18}O and ^{16}O isotopes within each of experimental samples remain constant. This condition can be disturbed only by the evaporation or loss of volatiles or alkalis at high temperatures There was no volatiles and alkalis in our compositions, and the temperature was lower than needed for evaporation of silicate melts. Thus, the heavy oxygen content in each melt drop suspended on a loop can be described by the following equation:

$$\delta^L = \delta_{nb}X_{nb} + \delta_bX_b + \delta_fX_f, \quad (2)$$

where subscript indices nb, b, and f denote non-bridging (O^-), bridging (O^0), and free (O^{2-}) oxygen, δ is the $\delta^{18}O$ value typical of corresponding type of oxygen, X is the mole fraction of the corresponding oxygen types in the melt (nb, b, f). If content of free oxygen O^{2-} is low (i.e., $f \to 0$), the last term of equation (2) can be ignored, while X_b can be expressed through the difference:

$$X_b = 1 - X_{nb}. \quad (3)$$

At isotope equilibration with gas (for instance, with O_2 of ambient atmosphere), the equilibrium distribution of ^{18}O isotope in a definite structural position (Si–O–Si—bridging, Si–O–M—non-bridging) is controlled by the following reactions of isotope exchange:

$$Si–O–Si + OO^* \leftrightarrow Si–O^*–Si + O_2, \quad (4a)$$

$$Si–O–M + OO^* \leftrightarrow Si–O^*–M + O_2, \quad (4b)$$

where O and O* are ^{16}O and ^{18}O, respectively. The oxygen isotope fractionation coefficients for reactions (4a, 4b) can be written as follows:

$$\alpha_{b\text{-}a} = R_b/R_a, \quad (5a)$$

$$\alpha_{nb\text{-}a} = R_{nb}/R_a, \quad (5b)$$

where $R_{nb,}$ R_b is the isotope ratio ($^{18}O/^{16}O$) in non-bridging and bridging oxygens, respectively, while R_a is oxygen in the ambient atmosphere. Combination of equations (5a) and (5b) yields the equation of fractionation coefficient through bridging and non-bridging oxygens:

$$\alpha_{b\text{-}nb} = R_b/R_{nb} = (1000 + \delta_b)/(1000 + \delta_{nb}). \quad (6)$$

In the first approximation, the following equation is fulfilled for high-temperature isotope fractionation:

$$10^3 Ln\alpha_{b\text{-}nb} \approx \delta_b - \delta_{nb} = \Delta_{b\text{-}nb}.$$

Therefore, the isotope composition of non-bridging oxygen can be written as the difference:

$$\delta_{nb} = \delta_b - \Delta_{b\text{-}nb}\,. \quad (7)$$

The oxygen isotope composition of melt, δ(L), that is in equilibrium with ambient gas can be deduced from mass balance equations (2) and (6), (7):

$$\delta(L) = \delta_{nb}X_{nb} + \delta_bX_b,$$
$$\delta(L) = \delta_b(L) - X_{nb}(L)\Delta_{b\text{-}nb} \quad (8)$$
$$\text{or } \delta(L) = \delta_b(L) - X_{nb}(L)\times 10^3 Ln\alpha_{b\text{-}nb},$$

because $\delta_b - \delta_{nb} \approx 10^3 Ln\alpha_{b\text{-}nb}$.

Equation (8) indicates that any melt (L1, L2, L3, etc.) which are in equilibrium with the same gas define linear correlation between $\delta^{18}O$ of the melt and X_{nb}, if $\alpha_{b\text{-}nb}$ does not depend (or weakly depends) on the

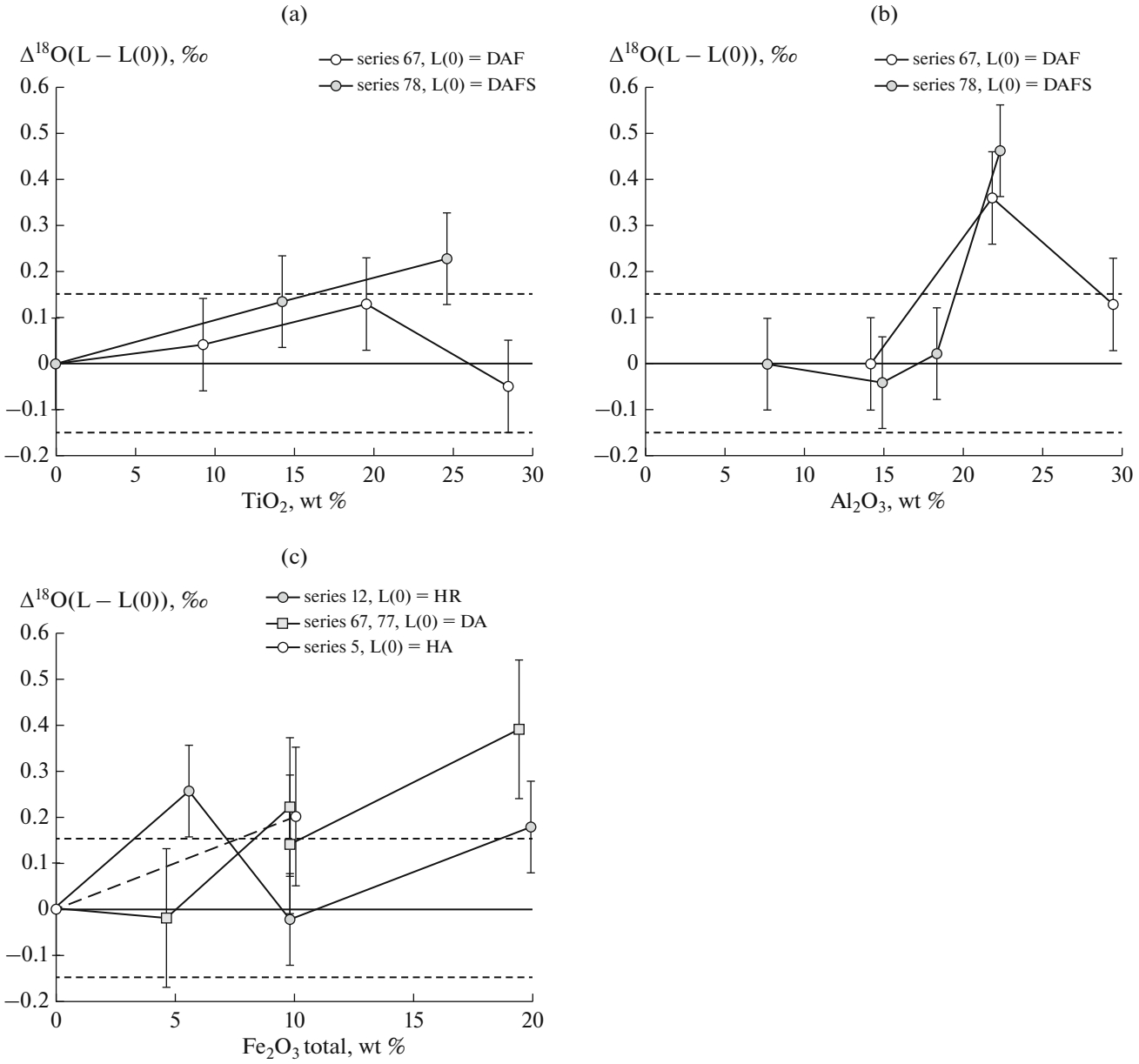

Fig. 4. Oxygen isotope fractionation relative to the starting composition (L(0)), owing to addition of oxides of network-forming cations: (a) titanium, (b) aluminum, (c) iron. Dashed lines denote interval given by analytical error.

chemical composition of the melt. The slope of regression line defined by equation (8) in the diagram X_{nb}–$\delta^{18}O(L)$ will be equal ($10^3 Ln\alpha_{b\text{-}nb}$), while the intersection with *y*-axis will define $\delta_b(L)$—the isotope composition of bridging oxygen in equilibrium with ambient gas.

Our experimental data were obtained using uniform internal standard (DA) with oxygen isotope composition ($\delta(DA)$) which can be expressed by equation similar to (8):

$$\delta(DA) = \delta_b(DA) - X_{nb}(DA) \times 10^3 Ln\alpha_{b\text{-}nb}. \quad (9)$$

Isotope fractionation $\Delta^{18}O(L{-}DA)$ in a melt L relative to DA can be obtained by subtraction of (9) from (8):

$$\Delta^{18}O(L\text{-}DA) = \delta_b(L) - \delta_b(DA) - 10^3 Ln\alpha_{b\text{-}nb}[X_{nb}(L) - X_{nb}(DA)]. \quad (10)$$

If the accepted assumptions are true, all experimental data points on the $\Delta^{18}O(L\text{-}DA)$–$[X_{nb}(L) - X_{nb}(DA)]$ diagram would be grouped along a straight line. As follows from equation (10), the slope of this line would be equivalent to $10^3 Ln\alpha_{b\text{-}nb}$ ($\approx\Delta_{b\text{-}nb}$). If the isotope composition of bridging oxygen in equilibrium

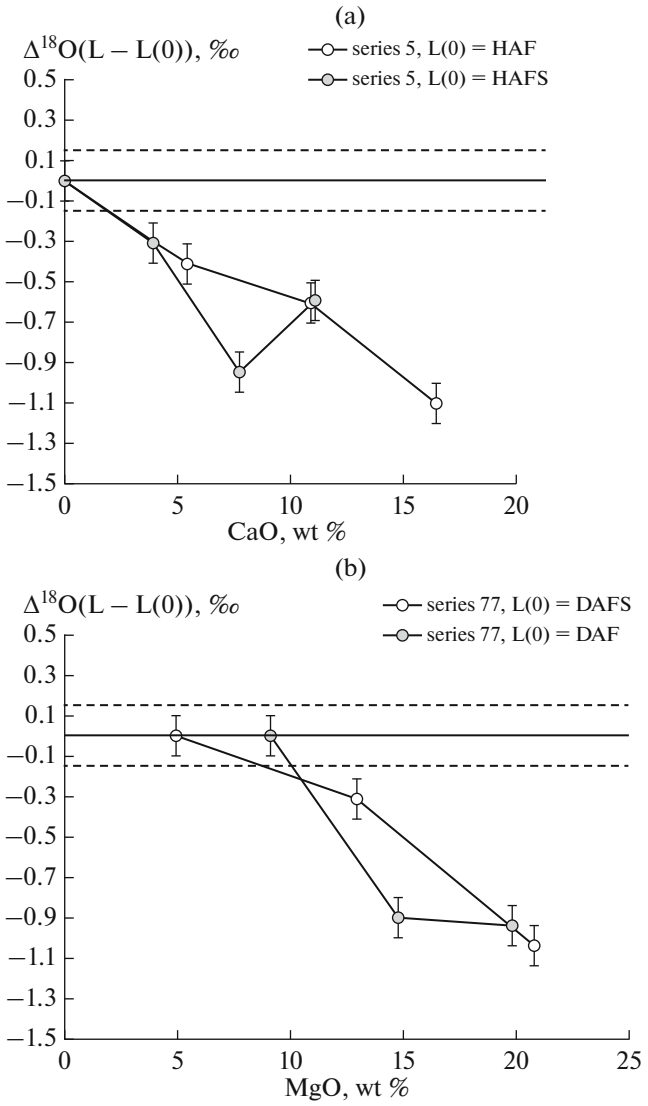

Fig. 5. Oxygen isotope fractionation relative to the starting composition (L(0)), owing to addition of modifier cations: calcium (a) and magnesium (b). Dash denotes interval defined by analytical error.

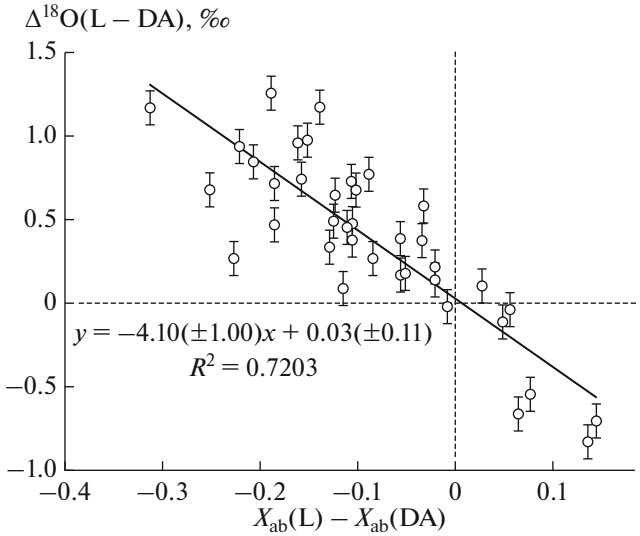

Fig. 6. Oxygen isotope fractionation in silicate melts relative to the melt of diopside–anorthite eutectic (DA) composition depending on the content of non-bridging oxygen (X_{nb}) in a melt (L) and base eutectics (DA).

with the same gas does not depend on the chemical composition and is similar for all coexisting melts, this line would pass through the origin. So, when the $\delta_b(L) = \delta_b(DA)$ the equation (10) transforms into:

$$\Delta^{18}O(L\text{-}DA) = -10^3 Ln\alpha_{b\text{-}nb}[X_{nb}(L) - X_{nb}(DA)]. \quad (11)$$

On the diagram $\Delta^{18}O(L\text{-}DA) - [X_{nb}(L) - X_{nb}(DA)]$ all obtained in this work experimental data are collected (Fig. 6). The experimental points show a good correlation ($R^2 = 0.72$, $n = 39$), and zero intersection with y-axis (0.03 ± 0.11), according to equation (11). Intersection of experimental trend with the origin denotes that $\delta^{18}O$ values of bridging oxygen in different melts are similar, in spite of significant variations of network-forming cations in these melts. For example, the SiO_2/Al_2O_3 mole ratio varies from 2.1 to 15.3, while the SiO_2/TiO_2 ratio varies from 1.4 to 11.4 (Table 1). A slope of correlation line in Fig. 6 allow to estimate $10^3 Ln\alpha_{b\text{-}nb} = 4.19$ (± 1.02), which corresponds to the fractionation factor between bridging and non-bridging oxygen ($\alpha_{b\text{-}nb}$) is 1.0042 (± 0.0010). Thus, experimentally estimated difference between $\delta^{18}O$ values of bridging and non-bridging oxygens (intra-structure fractionation) in silicate melts is 4.2 ± 1‰ at 1500 °C.

Further experiments need to clarify the temperature influence, which likely is complex. The reason is a poor known dependence of X_{nb} (as NBO/T ratio) on temperature (Mysen, 1997 etc.). Since the oxygen isotope fractionation in silicate melts is controlled by the fraction of non-bridging oxygen and value of intra-structure fractionation, it is difficult to predict the exact values of oxygen fractionation coefficient at other temperatures. However, in general form this dependence could be derived assuming that the intra-structure fractionation of oxygen isotopes is analogical to the usual equilibrium fractionation coefficients. In this case, $\Delta_{b\text{-}nb}$ is described by equation:

$$\Delta_{b\text{-}nb} \approx 10^3 Ln\alpha_{b\text{-}nb} = A_{b\text{-}nb} \times 10^6 T^{-2}. \quad (12)$$

To write the oxygen isotope fractionation between two silicate melts L and L' in general form the equations (12) and (11) should be combined:

$$\Delta^{18}O(L - L') = -A_{b\text{-}nb} \times 10^6 T^{-2}(X^T_{nb}(L) - X^T_{nb}(L')). \quad (13)$$

The equation (13) shows that the oxygen isotope fractionation between silicate melt and reference phase (for example, other silicate melt of definite

composition) may depend on not only temperature, but also on proportions of oxygens in different structural positions. The equation (13) is constrained by the negligible mole fraction of free (O^{2-}) oxygen in a melt, X_f. Hence, to describe the melts with the low content of network-forming cations (for example, with SiO_2 content less than 40 wt %), this equation has to be complicated to take into account the isotope fractionation for free oxygen in a melt. This requires further experimental studies. The application of this equation is also limited if L and L' are highly polymerized melts with extremely low content of non-bridging oxygen.

CONCLUSIONS

Our studies showed that significant isotope fractionation in silicate melts can be observed even in high-temperature region. Proposed explanation of experimental data using the mass-balance calculations suggests that oxygen isotope fractionation in silicate melts is determined by structural position of oxygen atoms and intra-structure isotope fractionation which is $4.2 \pm 1‰$ at 1500°C.

As the statistical threatment demonstrate, oxygen isotope fractionation in melts relative to the reference DA (diopside–anorthite eutectics) at 1500°C is clearly related to the NBO/T ($R^2 = 0.75$) and mole fraction of non-bridging oxygen X_{nb} ($R^2 = 0.73$). The chemical indices (Garlick, λ_{th}, λ_{corr}, $I^{18}O$) show a weak correlation with oxygen isotope fractionation (R^2 from 0.31 to 0.57). Thus, obtained results can be explained by the simple model of silicate melt structure. It is highly probable that using the more perfect but more complex models of silicate melt structure could lead to the revision of our estimations. However, available experimental results can be reasonably explained through oxygen isotope fractionation between its structural types (bridging and non-bridging oxygens) in a melt.

One of the main results of this work is the confirmation of previous assumption (Borisov and Dubinina, 2014) that the NBO/T ratio provides the better approximation of chemical composition of a melt than traditionally applied parameters (Garlick index, $I^{18}O$ index). The obtained results can be used in studying the isotope effects in systems with limited miscibility of melts. At the same time, our results can be also applied in solving of many petrological problems. For example, oxygen isotope fractionation in the phenocryst–lava system may demonstrate more complex behavior than previously considered. This is of great importance for basic and ultrabasic melts, because oxygen isotope fractionation coefficients are able to vary depending on the polymerization degree, which can be significantly changed during fractional crystallization.

ACKNOWLEDGMENTS

We are grateful to S.A. Kossova (IGEM RAS) for help in the performance of oxygen isotope analysis. We are thankful to V.B. Polyakov (IEM RAS) and A. A. Ariskin (GEOKhI RAS) for constructive discussion of the results of our work.

The work is a part of the RSF project 18-17-00126. This work was also partially supported by RFBR project 15-05-04716 ended in 2017.

REFERENCES

Anfilogov, V.N., Bykov, V.N., and Osipov, A.A., *Silikatnye rasplavy* (Silicate Melts), Moscow: Nauka, 2005.

Appora, I., Eiler, J.M., Matthews, A., and Stolper, E.M., Experimental determination of oxygen isotope fractionations between CO_2 vapor and soda–melilite melt, *Geochim. Cosmochim. Acta,* 2003, vol. 67, pp. 459–471.

Ariskin, A.A. and Polyakov, V.B., Simulation of molecular mass distributions and evaluation of O^{2-} concentrations in polymerized silicate melts, *Geochem. Int.*, 2008, vol. 46, no. 5, pp. 429–447.

Bigeleisen, J. and Mayer, M.G., Calculation of equilibrium constants for isotope exchange reactions, *J. Chem. Phys.*, 1947, vol. 15, pp. 261–267.

Borisov, A., Loop technique: dynamic of metal/melt equilibration, *Mineral. Petrol.,* 2001, vol. 71, pp. 87–94.

Borisov, A.A. and Dubinina, E.O., Effect of network-forming cations on the oxygen isotope fractionation between silicate melts: experimental study at 1400–1570°C, *Petrology,* 2014, vol. 22, no. 4, pp. 359–380.

Borisov, A., Behrens, H., and Holtz, F., The effect of titanium and phosphorus on ferric/ferrous ratio in silicate melts: an experimental study, *Contrib. Mineral. Petrol.,* 2013, vol. 166, pp. 1577–1591.

Borisov, A., Behrens, H., and Holtz, F., Effects of melt composition on Fe^{3+}/Fe^{2+} in silicate melts: a step to model ferric/ferrous ratio in multicomponent systems, *Contrib. Mineral. Petrol.,* 2015, vol. 169.

Borisov, A., Behrens, H., and Holtz, F., Effects of strong network modifiers on Fe^{3+}/Fe^{2+} in silicate melts: an experimental study, *Contrib. Mineral. Petrol.,* 2017, vol. 172.

Bucholz, C.E., Jagoutz, O., Van Tongeren, J.A., et al., Oxygen isotope trajectories of crystallizing melts: insights from modeling and the plutonic record, *Geochim. Cosmochim. Acta,* 2017, vol. 207, pp. 154–184.

Canil, D. and Muehlenbachs, K., Oxygen diffusion in an Fe-rich basalt melt, *Geochim. Cosmochim. Acta,* 1990, vol. 54, pp. 2947–2951.

Chacko, T., Cole, D.R., and Horita, J., Equilibrium oxygen, hydrogen and carbon isotope fractionation factors applicable to geological systems, *Rev. Mineral.,* 2001, vol. 43, pp. 1–81.

Clayton, R.N. and Kieffer, S.W., Oxygen isotope thermometer calibrations, *Stable Isotope Geochemistry: A Tribute to Samuel Epstein,* Taylor, H.P., Jr, O'Neil, J.R., Kaplan, I.R., Eds., *Geochem. Soc. Spec. Publ.,* 1991, no. 3, pp. 3–10.

Coplen, T.B., Reporting of stable hydrogen, carbon, and oxygen isotopic abundances, *Pure Appl. Chem.,* 1994, vol. 66, pp. 273–276.

Dalou, C., Le Losq, C., and Mysen, B.O., In situ study of the fractionation of hydrogen isotopes between aluminosilicate melts and coexisting aqueous fluids at high pressure and high temperature: implications for the δD in magmatic processes, *Earth Planet. Sci. Lett.,* 2015, vol. 426, pp. 158–166.

Duffy, J.A., A review of optical basicity and its applications to oxidic systems, *Geochim. Cosmochim. Acta,* 1993, vol. 57, pp. 3961–3970.

Dunn, T., Oxygen diffusion in three silicate melts along the join diopside–anorthite, *Geochim. Cosmochim. Acta,* 1982, vol. 46, pp. 2293–2299.

Eiler, J.M., *Oxygen isotope variations of basaltic lavas and upper mantle rocks, Stable Isotope Geochemistry*, Valley, J.W. and Cole, D.R., Eds., *Rev. Mineral,* 2001, vol. 43, pp. 319–364.

Esin, O.A. Polymineral model of melted silicates, in *Solutions. Melts: Results of Science and Technique,* Moscow: VINITI, 1975, vol. 2, pp. 76–107.

Fincham, C.J.B. and Richardson, F.D., The behavior of sulfur in silicate and aluminate melts, *Proc. R. Soc. London: Ser. A,* 1954, vol. 223.

Garlick, G.D., Oxygen isotope fractionation in magmatic rocks, *Earth Planet. Sci. Lett.,* 1966, vol. 1, pp. 361–368.

Hao, X. and Wang, X., A new sulfide capacity model for $CaO–Al_2O_3–SiO_2–MgO$ slags based on corrected optical basicity, *Steel Res. Intern.,* 2017, vol. 87, pp. 359–363.

Hess, P.C., Polymer model of silicate melts, *Geochim. Cosmochim. Acta,* 1971, vol. 36, pp. 289–306.

Kroopnick, P. and Craig, H., Atmospheric oxygen: isotopic composition and solubility fractionation, *Science,* 1972, vol. 175, pp. 54–55.

Kyser, T.K., Lesher, C.E., and Walker, D., The effects of liquid immiscibility and thermal diffusion on oxygen isotopes in silicate liquids, *Contrib. Mineral. Petrol.,* 1998, vol. 133, pp. 373–381.

Labidi, J., Shahar, A., Le Losq, C., et al. Experimentally determined sulfur isotope fractionation between metal and silicate and implications for planetary differentiation, *Geochim. Cosmochim. Acta,* 2016, vol. 175, pp. 181–194.

Lesher, C.E., Self-diffusion in silicate melts: theory, observations and applications to magmatic systems, *Rev. Mineral. Geochem.,* 2010, vol. 72, pp. 269–309.

Lester, G.W., Kyser, T.K., and Clark, A.H., Oxygen isotope partitioning between immiscible silicate melts with H_2O, P and S, *Geochim. Cosmochim. Acta,* 2013, vol. 109, pp. 306–311.

Le Losq, C., Mysen, B.O., and Cody, G.D., Intramolecular fractionation of hydrogen isotopes in silicate quenched melts, *Geochem. Persp. Lett.,* 2016, vol. 2, pp. 87–94.

Masson, C.R., Ionic equilibria in liquid silicates, *J. Am. Ceram. Soc.,* 1968, vol. 51, pp. 134–143.

Masson, C.R., Smith, I.B., and Whiteway, S.G., Activities and ionic distributions in liquid silicates: application of polymer theory, *Can. J. Chem.,* 1970, vol. 48, pp. 1456–1464.

Matthews, A., Palin, J.M., Epstein, S., and Stolper, E.M., Experimental study of $^{18}O/^{16}O$ partitioning between crystalline albite, albitic glass and CO_2 gas, *Geochim. Cosmochim. Acta,* 1994, vol. 58, pp. 5255–5266.

Mills, K.C., The influence of structure on the physicochemical properties of slags, *ISIJ Int.,* 1993, vol. 33, pp. 148–155.

Moretti, R., Polymerisation, basicity, oxidation state and their role in ionic modelling of silicate melts, *Ann. Geophys.,* 2005, vol. 48, pp. 583–607.

Muehlenbachs, K. and Kushiro, I., Oxygen isotope exchange and equilibrium of silicates with CO_2 and O_2, *Carnegie Inst. Wash. Yearbook,* 1974, vol. 73, pp. 232–236.

Mungall, J.E., Empirical models relating viscosity and tracer diffusion in magmatic silicate melts, *Geochim. Cosmochim. Acta,* 2002, vol. 66, pp. 125–143.

Mysen, B.O., Aluminosilicate melts: structure, composition and temperature, *Contrib. Mineral. Petrol.,* 1997, vol. 127, pp. 104–118.

Mysen, B.O., Hydrogen isotope fractionation between coexisting hydrous melt and silicate-saturated aqueous fluid: an experimental study in situ at high pressure and temperature, *Am. Mineral.,* 2013, vol. 98, pp. 376–386.

Mysen, B.O. and Richet, P., *Silicate Glasses and Melts: Properties and Structure,* Amsterdam: Elsevier, 2005.

Mysen, B.O. and Fogel, M.L., Nitrogen and hydrogen isotope compositions and solubility in silicate melts in equilibrium with reduced (N + H)-bearing fluids at high pressure and temperature: effects of melt structure, *Am. Mineral.,* 2010, vol. 95, pp. 987–999.

Mysen, B.O., Virgo, D., and Seifert, F.A., Relationships between properties and structure of aluminosilicate melts, *Am. Mineral.,* 1985, vol. 70, pp. 88–105.

Palin, J.M., Epstein, S., and Stolper, E., Oxygen isotope partitioning between rhyolitic glass/melt and CO_2: an experimental study at 550–950°C and 1 bar, *Geochim. Cosmochim. Acta,* 1996, vol. 60, pp. 1963–1973.

Qin, T., Wu, F., Wu, Z., and Huang, F., First principles calculations of equilibrium fractionation of O and Si isotopes in quartz, albite, anorthite and zircon, *Contrib. Mineral. Petrol.,* 2016, vol. 171, p. 91.

Schuessler, J.A., Botcharnikov, R.E., Behrens, H., et al., Oxidation state of iron in hydrous phono-tephritic melts, *Am. Mineral.,* 2008, vol. 93, pp. 1493–1504.

Sharp, Z.D., A laser-based microanalytical method for the in situ determination of oxygen isotope ratios in silicates and oxides, *Geochim. Cosmochim. Acta,* 1990, vol. 54, pp. 1353–1357.

Stolper, E. and Epstein, S., An experimental study of oxygen isotope partitioning between silica glass and CO_2 vapor, *Stable Isotope Geochemistry: A Tribute to Samuel Epstein*, Taylor, H.P., Jr, O'Neil, J.R, and Kaplan, I.R., Eds., *Geochem. Soc. Spec. Publ.,* 1991, vol. 3, pp. 35–51.

Toop, G.W. and Samis, C.S., Activities of ions in silicate melts, *Transactions of the Metallurgical Society of America,* 1962, vol. 224, pp. 878–887.

Valley, J.W., Kitchen, N., Kohn, M.J., et al., UWG-2, a garnet standard for oxygen isotope ratios: strategies for high precision and accuracy with laser heating, *Geochim. Cosmochim. Acta,* 1995, vol. 59, pp. 5223–5231.

Wang, Y., Cody, S.X., Foustoukos, D., et al., Very large differences in intramolecular D–H partitioning in hydrated silicate melts synthesized at upper mantle pressures and temperatures, *Am. Mineral.,* 2015, vol. 100, pp. 1182–1189.

Wendlandt, R.F., Oxygen diffusion in basalt and andesite melts: experimental results and discussion of chemical versus tracer diffusion, *Contrib. Mineral. Petrol.,* 1991, vol. 108, pp. 463–471.

Zhao, Z.F. and Zheng, Y.F., Calculation of oxygen isotope fractionation in magmatic rocks, *Chem. Geol.,* 2003, vol. 193, pp. 59–80.

Zheng, Y.F., Calculation of oxygen isotope fractionation in metal oxides, *Geochim. Cosmochim. Acta,* 1991, vol. 55, pp. 2299–2307.

Zheng, Y.F., Calculation of oxygen isotope fractionation in anhydrous silicate minerals, *Geochim. Cosmochim. Acta,* 1993, vol. 57, pp. 1079–1091.

Translated by M. Bogina